Robotica (2013) volume 31, pp. 969–980. © Cambridge University Press 2013
doi:10.1017/S0263574713000210

Calibration of omnidirectional wheeled mobile robots: method and experiments

Yaser Maddahi†, Ali Maddahi‡ and Nariman Sepehri†*

† *Department of Mechanical Engineering, University of Manitoba, Winnipeg, MB, Canada, R3T 5N5*
‡ *Department of Mechanical Engineering, K. N. Toosi University of Technology, Tehran, Iran*

(Accepted February 24, 2013. First published online: April 11, 2013)

SUMMARY

Odometry errors, which occur during wheeled mobile robot movement, are inevitable as they originate from hard-to-avoid imperfections such as unequal wheels diameters, joints misalignment, backlash, slippage in encoder pulses, and much more. This paper extends the method, developed previously by the authors for calibration of differential mobile robots, to reduce positioning errors for the class of mobile robots having omnidirectional wheels. The method is built upon the easy to construct kinematic formulation of omnidirectional wheels, and is capable of compensating both systematic and non-systematic errors. The effectiveness of the method is experimentally investigated on a prototype three-wheeled omnidirectional mobile robot. The validations include tracking unseen trajectories, self-rotation, as well as travelling over surface irregularities. Results show that the method is very effective in improving position errors by at least 68%. Since the method is simple to implement and has no assumption on the sources of errors, it should be considered seriously as a tool for calibrating omnidirectional mobile having any number of wheels.

KEYWORDS: Omnidirectional wheeled mobile robots; Systematic errors; Non-systematic errors; Benchmark tests; Error improvement; Performance analysis.

1. Introduction

Wheeled mobile robots (WMRs) are found in many applications such as planetary exploration and surveillance operations. The shape, dimension, and properties of WMRs are usually specified by some input parameters during the design process. Wheels used in WMRs belong to one of the three types: standard, castor, or omnidirectional (see Fig. 1).

Standard wheels are powered to permit the robot to move. They are simple to build and have good reliability. Castor wheels are used along with the standard wheels to facilitate balancing of the robot. They are capable of steering around their vertical axes. Omnidirectional wheels, on the other hand, are capable of acting as both castor and standard wheels. Various types of omnidirectional mobile robots have been reported in the literature such as universal wheels,[1,2] ball wheels,[3] and off-centered wheels.[4] Mobile robots with omnidirectional wheels are controllable with reduced number of actuators, and are highly maneuverable in narrow or crowded spaces.

Accuracy of motion in omnidirectional wheeled mobile robots (OWMRs) is influenced by two types of errors: systematic and non-systematic. Systematic errors are caused by unavoidable imperfections in the control and mechanical subsystems such as misalignment and friction in joints. Non-systematic errors are caused by unpredictable phenomena such as wheel slippage and surface irregularities. Both systematic and non-systematic errors are needed to be reduced or the robot should be calibrated to achieve reasonable positioning errors.

Calibration is defined as a set of operations that establishes, under specified conditions, the relationship between the values of quantities indicated by a measuring instrument and the corresponding values realized by standards.[5] The calibration approaches, used for calibrating WMRs, include odometry,[6] 3D camera error detection,[7] active beacons,[8] gyroscope,[9] and magnetic compasses.[10] Odometry uses data from the movement of actuators to estimate change in position over time. As compared with other methods, odometry provides a better short-term accuracy allowing very high sampling rates at low cost.[11,12] The odometry method can be applied to correct errors of all types of WMRs. As far as previous work on odometry applied to WMRs is concerned, Borenstein and Feng[13–15] introduced a method for measuring odometry errors of differential drive mobile robots. This method was called University of Michigan Benchmark (UMBmark). They implemented the UMBmark method to correct both systematic and non-systematic errors for the class of differential drive mobile robots in which two independent standard wheels are actively controlled. Maddahi and Maddahi[6] and Maddahi[16] applied the UMBmark method on different types of differential drive mobile robots and proposed a new odometry method to correct systematic errors of differential drive mobile robots.[12] By applying their method, which is built upon the robot kinematics, on six prototyped differential drive WMRs, it was confirmed that the proposed method is simpler and requires less time to perform the calibration as compared with the UMBmark method. The only literature identified by the authors that relates to odometry-based calibration of OWMRs belongs to Han *et al.*[17] They identified three sources of position errors in OWMRs: the slippage between the wheel and the

* Corresponding author. E-mail: nariman.sepehri@ad.umanitoba.ca

https://doi.org/10.1017/S0263574713000210 Published online by Cambridge University Press

(a) Standard wheel (b) Castor wheel (c) Omnidirectional wheel

Fig 1. (Colour online) Schematic view of various wheel types used in mobile robots.

floor surface, the mechanical effects of sub-roller bearings and/or axles, and the rotational friction at the wheel contact point. A simple calibration equation on the Cartesian velocity elements was also developed.[17] Other sources of errors such as uncertainty in wheels diameters and differences in wheel diameters were not considered in their work.

This paper extends the previous work by the authors[12] to calibrate errors in OWMRs having both types of systematic and non-systematic errors. The method presented here is built upon the kinematic equations of omnidirectional robots. Using this method, the robot is programmed to move along a straight trajectory. The measured position errors with respect to the desired destination are used within the kinematic equations, and values of two corrective indices are determined to properly correct the robot's future movements. The indices are: (i) lateral corrective matrix, which compensates the lateral position error, and (ii) longitudinal corrective factor, which eliminates the robot longitudinal position error. As compared with the previous study by the authors,[12] the current method is applied to a different class of mobile robot types for the first time. It is also constructed symbolically facilitating its application to WMRs with different number of wheels (standard or omnidirectional). As compared with the work by Han *et al.*,[17] which was designed only to correct a limited number of error sources, the proposed method uses symbolic kinematic equations that helps the robot reduce position errors regardless of error sources. The proposed method is offline and should be considered as the first step in the calibration process to correct positioning errors. It can be further augmented by online calibration to achieve higher accuracy.[18–21]

The organization of this paper is as follows. Section 2 describes the kinematic formulation of OWMRs. Section 3 documents the proposed calibration method. The electromechanical description of the prototyped omnidirectional robot is described in Section 4, followed by the experimental results and corresponding validations, which include testing the robot along unseen double-square, double-triangular, combined straight, and curved trajectories as well as rotation around central axis (self-rotation). Section 5 outlines conclusions and future work.

2. Kinematic Modelling

In order to obtain the corrective indices for proper trajectory following, the proposed odometry method requires kinematic formulation describing the contribution of each omnidirectional wheel on movement. The kinematic diagram of a general three-wheeled omnidirectional robot is illustrated in Fig. 2(a). The total dimensionality of the mobile robot on the horizontal plane is three: two for position (x and y) and one for orientation (θ) of robot. Figure 2(b) shows a typical wheel and associated parameters. Each wheel rotates independently. The coordinate frames $X_R Y_R$ and $X_b Y_b$ define the global (reference) and base frames, respectively.

In an omnidirectional wheel, there is pure rolling at the contact point between the roller and the ground (non-slip condition). This constraint is formulated by applying the non-slip condition as follows[22]:

$$[\sin(\alpha_i + \beta_i + \gamma_i) \quad -\cos(\alpha_i + \beta_i + \gamma_i) \quad -l_i \cos(\beta_i + \gamma_i)]$$
$$R(\theta)\dot{\vec{\mu}} - r_i \dot{\varphi}_i \cos\gamma_i = 0. \tag{1}$$

The non-slip condition implies that the motion along the roller axis must be equal to the motion accomplished by spinning the wheel, $r_i \dot{\varphi}_i \cos\gamma_i$,[22] where i is the number of wheels. The first term in Eq. (1) denotes the total motion along the axis of roller. The three elements of the vector represent the mapping from $\dot{x}$, $\dot{y}$, and $\dot{\theta}$ to corresponding contribution along the roller axis. Term $R(\theta)\dot{\vec{\mu}}$ is used to transform the motion parameters in the Cartesian coordinate frame, $X_R Y_R$, into motion parameters in the base frame, $\{X_b Y_b\}$. This transformation is considered because all wheel parameters in Eq. (1) (β_i, γ_i, l_i, and α_i) are measured with respect to the base frame. β_i denotes the steering angle (angle of wheel plane relative to the robot main body), which is commonly constant. γ_i represents the angle between the main wheel plane and the axis of rotation of the small circumferential rollers. l_i is the distance from the geometrical center of the robot to the center of the wheel (wheelbase). α_i is the angle between the wheel shaft and X_R axis when the robot is at home position. $\dot{\varphi}$ and r are the angular velocity and the radius of the wheel, respectively. Matrix $R(\theta)$, which is a function of orientation angle (θ), is defined as follows:

$$R(\theta) = \begin{bmatrix} \cos\theta & \sin\theta & 0 \\ -\sin\theta & \cos\theta & 0 \\ 0 & 0 & 1 \end{bmatrix}. \tag{2}$$

Finally, $\dot{\vec{\mu}}$ is the robot velocity vector (linear and angular velocities) with respect to reference coordinate $X_R Y_R$,

https://doi.org/10.1017/S0263574713000210 Published online by Cambridge University Press

$$\vec{\mu} = \begin{bmatrix} \dot{x} & \dot{y} & \dot{\theta} \end{bmatrix}^T . \tag{3}$$

The general form of Eq. (1), for an omnidirectional mobile robot having n wheels, can be presented in following form:

$$\vec{\dot{\Phi}} = J^{-1}\vec{\mu}, \tag{4}$$

where the wheel velocity vector, $\vec{\dot{\Phi}}$, is defined as follows:

$$\vec{\dot{\Phi}} = [\dot{\varphi}_1 \quad \dot{\varphi}_3 \quad \dots \quad \dot{\varphi}_n]^T . \tag{5}$$

By comparing Eqs. (1) and (4), for an omnidirectional mobile robot with n wheels, the nominal inverse Jacobian matrix, $J^{-1}_{n\times 3}$, is obtained as follows:

$$J^{-1}_{n\times 3} = diag\left[\frac{1}{r_1\cos\gamma_1} \cdots \frac{1}{r_n\cos\gamma_n}\right]\begin{bmatrix} \sin(\alpha_1+\beta_1+\gamma_1) & -\cos(\alpha_1+\beta_1+\gamma_1) & -l_1\cos(\beta_1+\gamma_1) \\ \vdots & \vdots & \vdots \\ \sin(\alpha_n+\beta_n+\gamma_n) & -\cos(\alpha_n+\beta_n+\gamma_n) & -l_n\cos(\beta_n+\gamma_n) \end{bmatrix} R(\theta). \tag{6}$$

For a three-wheeled omnidirectional mobile robot ($n = 3$), for example, the nominal inverse Jacobian matrix ($J^{-1}_{n\times 3}$) is obtained by defining $\alpha_1 = \pi/2$, $\alpha_2 = 7\pi/6$, and $\alpha_3 = 11\pi/6$,

$$J^{-1}_{3\times 3} = \begin{bmatrix} \frac{1}{r_1\cos\gamma_1} & 0 & 0 \\ 0 & \frac{1}{r_2\cos\gamma_2} & 0 \\ 0 & 0 & \frac{1}{r_3\cos\gamma_3} \end{bmatrix}\begin{bmatrix} \sin(\frac{\pi}{2}+\beta_1+\gamma_1+\theta) & -\cos(\frac{\pi}{2}+\beta_1+\gamma_1+\theta) & -l_1\cos(\beta_1+\gamma_1) \\ \sin(\frac{7\pi}{6}+\beta_2+\gamma_2+\theta) & -\cos(\frac{7\pi}{6}+\beta_2+\gamma_2+\theta) & -l_2\cos(\beta_2+\gamma_2) \\ \sin(\frac{11\pi}{6}+\beta_3+\gamma_3+\theta) & -\cos(\frac{11\pi}{6}+\beta_3+\gamma_3+\theta) & -l_3\cos(\beta_3+\gamma_3) \end{bmatrix}. \tag{7}$$

3. Proposed Calibration Method

Figure 3 illustrates the defined trajectory and related variables for the proposed calibration method. With reference to Fig. 3, the robot is directed to move along the desired straight line (trajectory A) in Cartesian coordinate frame$\{X_R Y_R\}$. Due to various errors (systematic or non-systematic) and regardless of the sources, the robot follows a different trajectory (trajectory B). As shown in Fig. 3, the position error consists of two lateral and longitudinal error components. For calibration purpose, we define two corrective indices, namely lateral corrective matrix and longitudinal corrective factor.

The lateral corrective matrix (F_{lat}) is applied to kinematic equations of robot to ensure that the robot stays along the desired trajectory. This matrix is calculated using nominal ($\vec{\dot{\Phi}}$) and error-driven ($\vec{\dot{\Phi}}_e$) wheel angular velocities based on the error angle θ_e, measured during the test (see Fig. 3). Using Eq. (4), the error-driven wheels' angular velocity vector ($\vec{\dot{\Phi}}_e$) is calculated using the following formulation:

$$\vec{\dot{\Phi}}_e = J^{-1}\vec{\mu}_e \tag{8}$$

or

$$\begin{bmatrix} \dot{\varphi}_{e,1} \\ \dot{\varphi}_{e,2} \\ \vdots \\ \dot{\varphi}_{e,n} \end{bmatrix} = J^{-1}\begin{bmatrix} 0 \\ 0 \\ -\dot{\theta}_e \end{bmatrix}. \tag{9}$$

In Eq. (9), $\dot{\varphi}_{e,i}(i = 1, 2, \dots, n)$ represents the angular velocity errors, which should be added to the wheel nominal angular velocity $\dot{\varphi}_i(i = 1, 2, \dots, n)$. $\dot{\theta}_e$ is obtained by dividing the measured error angle, θ_e, to the time taken for the robot to travel the entire trajectory B. Note that θ_e is measured using a protractor tool and the robot is commanded to move at a constant speed.

The lateral corrective matrix, F_{lat}, which constrains the robot to move along the desired straight trajectory (trajectory A), is now expressed as follow:

$$F_{lat} = diag\left[1 + \frac{\dot{\varphi}_{e,1}}{\dot{\varphi}_1} \cdots 1 + \frac{\dot{\varphi}_{e,n}}{\dot{\varphi}_n}\right]. \tag{10}$$

By applying the lateral corrective matrix to equations of omnidirectional robot, the error angle, θ_e, becomes small, i.e., the robot maintains to stay along trajectory A. However, even if the robot is aligned with the desired trajectory, it is still required to reach the desired location, i.e., having no longitudinal error. This is done by defining longitudinal corrective factor (F_{lon}), which compensates the robot's longitudinal position error occurring along trajectory A. F_{lon} is obtained by equally adjusting the speed of the wheels and defined as follows:

$$F_{\text{lon}} = \frac{L}{\sqrt{(L+\bar{x}_e)^2 + (\bar{y}_e)^2}}, \tag{11}$$

where L is the length of trajectory A, which is the distance between O_R and O^d_R, $\bar{x}_e = \frac{1}{N}\sum_{k=0}^{N}(x_{e,k})$, $\bar{y}_e = \frac{1}{N}\sum_{k=0}^{N}(y_{e,k})$, and N is the number of trial runs. Note that in Eq. (11), the denominator represents the length of the average actual trajectory travelled by the mobile robot over N trials. The significance of the proposed method is that it is built on simple and easy-to-understand kinematic equations. In addition, the method does not make any assumption on the sources of error in robot motion.

As described in this section, the proposed method compensates for the robot error using lateral corrective matrix (F_{lat}) and longitudinal corrective factor (F_{lon}). The most integrated approach to incorporate these indices in the robot equations of motion is to use them within Jacobian matrix that relates the robot trajectory variables (position and orientation) to the joints' (wheels) variables, as shown in Eq. (4). This relationship is expressed as follows:

$$\vec{\dot{\Phi}}_c = J_c^{-1}\vec{\dot{\mu}}. \tag{12}$$

In Eq. (12), $\vec{\dot{\Phi}}_c$ denotes that the corrected wheel angular velocity vector should be applied on motors to ensure the

https://doi.org/10.1017/S0263574713000210 Published online by Cambridge University Press

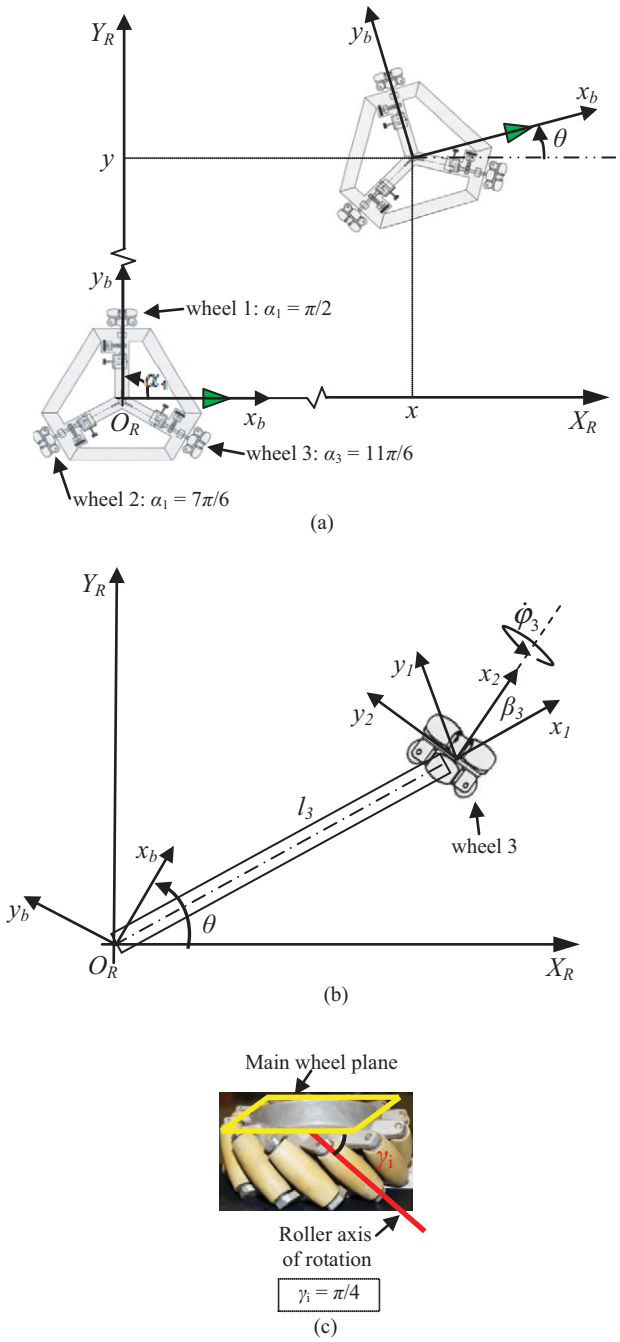

Fig 2. (Colour online) (a) Coordinate frames of three-wheeled omnidirectional mobile robot in 2D workspace; (b) close-up view of wheel 3 assembly. The generalized coordinate systems and parameters of the third wheel, including wheelbase (l_3), steering angle (β_3), and angular velocity ($\dot{\varphi}_3$) are shown in (b); (c) typical example of the angle between the main wheel plane and the roller axis of rotation (γ_i).

robot moves along the proper trajectory and reaches the desired destination. J_c^{-1} (corrected inverse Jacobian matrix) is expressed as follows:

$$J_c^{-1} = F_{\text{lon}} F_{\text{lat}} J^{-1} diag\left[\left(1+\frac{\dot{\varphi}_{e,1}}{\dot{\varphi}_1}\right)\frac{1}{r_1\cos\gamma_1}\cdots\left(1+\frac{\dot{\varphi}_{e,n}}{\dot{\varphi}_n}\right)\frac{1}{r_n\cos\gamma_n}\right]$$
$$\times\begin{bmatrix} F_{\text{lon}}\sin(\alpha_1+\beta_1+\gamma_1) & -F_{\text{lon}}\cos(\alpha_1+\beta_1+\gamma_1) & -F_{\text{lon}}l_1\cos(\beta_1+\gamma_1) \\ \vdots & \vdots & \vdots \\ F_{\text{lon}}\sin(\alpha_n+\beta_n+\gamma_n) & -F_{\text{lon}}\cos(\alpha_n+\beta_n+\gamma_n) & -F_{\text{lon}}l_n\cos(\beta_n+\gamma_n) \end{bmatrix} R(\theta), \quad (13)$$

where $\vec{\mu}$, F_{lat}, and F_{lon} are defined by Eqs. (3), (10), and (11), respectively. Also, J^{-1} is defined based on the omnidirectional mobile robot mechanism using Eq. (6).

The calibration steps based on the odometry method described above are summarized as follows:

i. Prepare the robot at a start position. Set orientation angle of omnidirectional mobile robot to zero.
ii. Run the vehicle through a straight trajectory, making sure to stop after a predetermined length of travelling.
iii. Upon completion of motion, measure the absolute position of the robot body with respect to the reference coordinate.
iv. Repeat steps (i) to (iii) for a number of times. The number of the tests depends on the expected positioning accuracy in calibration.
v. Calculate the lateral and longitudinal errors (x_e and y_e) and error angle (θ_e) of robot for each trial.
vi. Calculate the lateral corrective matrix (F_{lat}) and longitudinal corrective factor (F_{lon}) using Eqs. (10) and (11), respectively.
vii. Apply corrective indices to symbolic form of kinematic equation using Eqs. (12) and (13).

4. Experimental Results

4.1. Prototype robot

The prototype three-wheeled omnidirectional mobile robot was designed with high maneuverability. As shown in Fig. 4, the robot is composed of three omnidirectional driving wheels with their own transmission systems, which are independently driven by three DC motors. The omnidirectional wheels are centered on the longitudinal axis of the robot. These wheels are driven by non-steering wheels powered by independent mechanisms and have single-row roller arrangement. The axis of each wheel is parallel to the horizontal plane from the pivot point in the direction perpendicular to the wheel axis ($\beta_{1,2,3} = 0$). Also,

Table I. Specifications of prototype robot.

Specification	Dimension
Dimension (L × W × H)	29 × 29 × 12 cm^3
Weight	1.250 kg
Stall torque of drive motors	0.2 Nm
Maximum speed	7.30 m/min
Wheel radius	0.07 m
Wheelbase	0.138 m
Encoder resolution	360 pulse/rev
Wheel steering angle (β)	0°
Roller axis angle (γ)	0°

https://doi.org/10.1017/S0263574713000210 Published online by Cambridge University Press

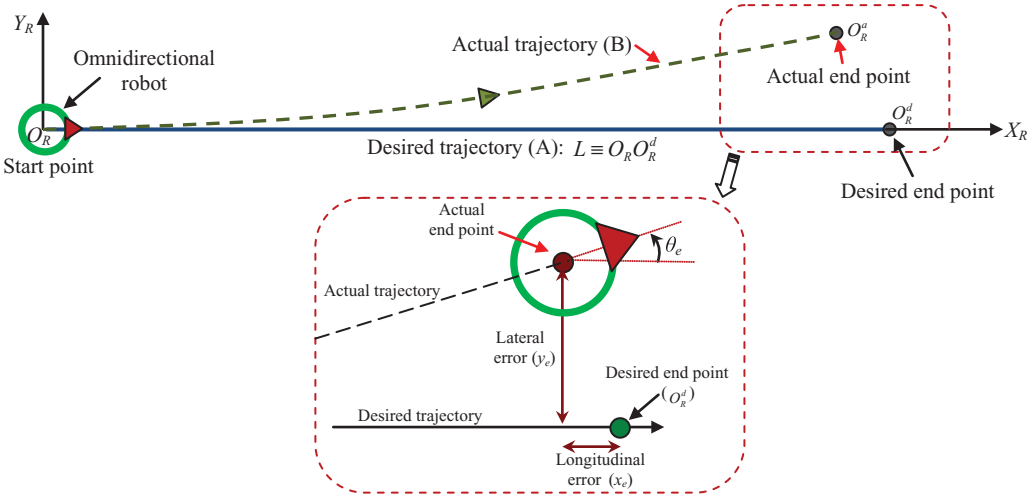

Fig 3. (Colour online) Trajectories in proposed method: desired trajectory (A); actual trajectory (B). Position error is measured with respect to desired end-point location O_R^d.

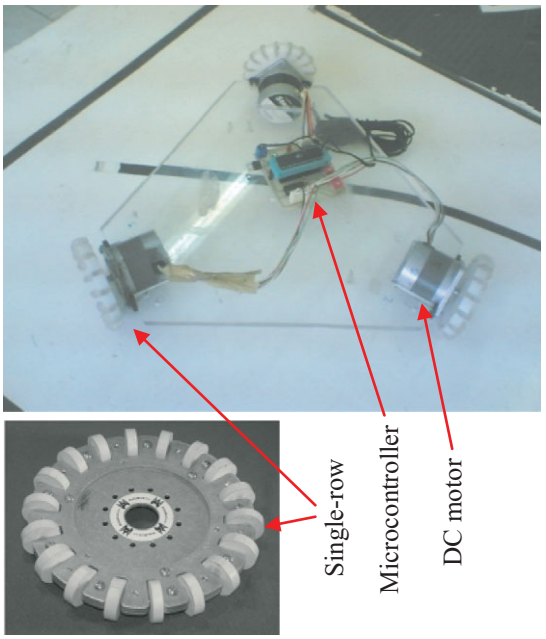

Fig 4. (Colour online) Prototype three-wheeled omnidirectional mobile robot.

the angle between rollers axis of rotation and wheel plane ($\gamma_{1,2,3} = 0$) is zero. Table I shows specifications of this prototyped robot.

4.2. *Evaluation criteria*

The index used to facilitate the comparison is the radial error (δr_e), which is defined as

$$\delta r_e = \frac{1}{N} \sum_{k=1}^{N} \sqrt{x_{e,k}^2 + y_{e,k}^2}, \tag{14}$$

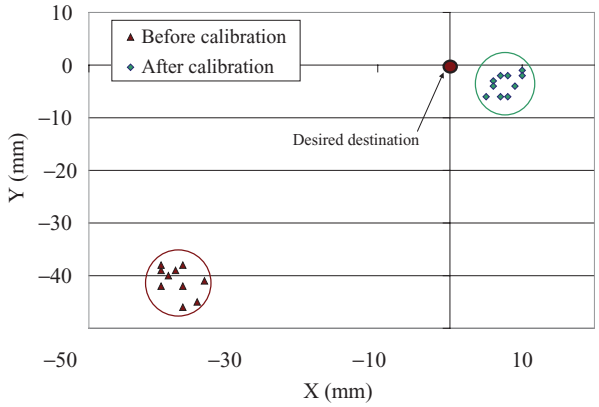

Fig 5. (Colour online) Radial systematic error of prototype three-wheeled OWMR before and after calibration.

where x_e and y_e are given in Fig. 3, and N represents the number of trial runs. The effectiveness of the proposed method is measured by comparing the mean error improvement index (δr_m):

$$\delta r_m = \frac{\left(\delta r_{e,\mathrm{BF}} - \delta r_{e,\mathrm{AF}}\right)}{\delta r_{e,\mathrm{BF}}} \times 100\% \tag{15}$$

where $\delta r_{e,\mathrm{BF}}$ and $\delta r_{e,\mathrm{AF}}$ are the mean values of radial errors before (BF) and after (AF) calibration, respectively.

4.3. *Calibration of systematic errors*

4.3.1. Calibration process. The method was applied to the robot, shown in Fig. 4, over 10 trial runs ($N = 10$). Figure 5 illustrates the position errors for the robot before and after calibration. In this test, the robot was programmed to travel along the x-axis. The initial configuration of robot,

Table II. Indices for systematic tests before (BF) and after (AF) calibration.

F_{lat}	F_{lon}	δr_e (mm)	δr_m	Kurtosis	Skewness
$diag\left[0.991\ 1.092\ 1.083\right]$	1.104	55.7 (BF) 8.7(AF)	84.38%	0.58 (BF) −0.23 (AF)	−0.24 (BF) −0.06 (AF)

https://doi.org/10.1017/S0263574713000210 Published online by Cambridge University Press

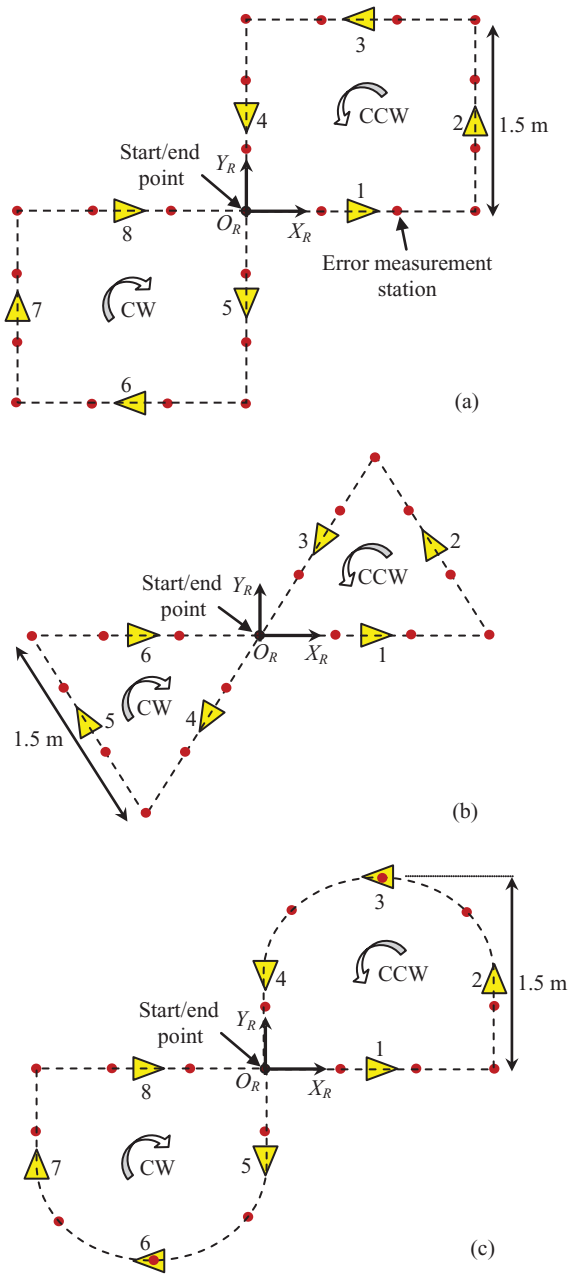

Fig 6. (Colour online) Unseen trajectories to test the performance of calibrated robot. Trajectories were designed to allow robot to move along three paths: (a) double-square, (b) double-triangular, and (c) combined straight and curved.

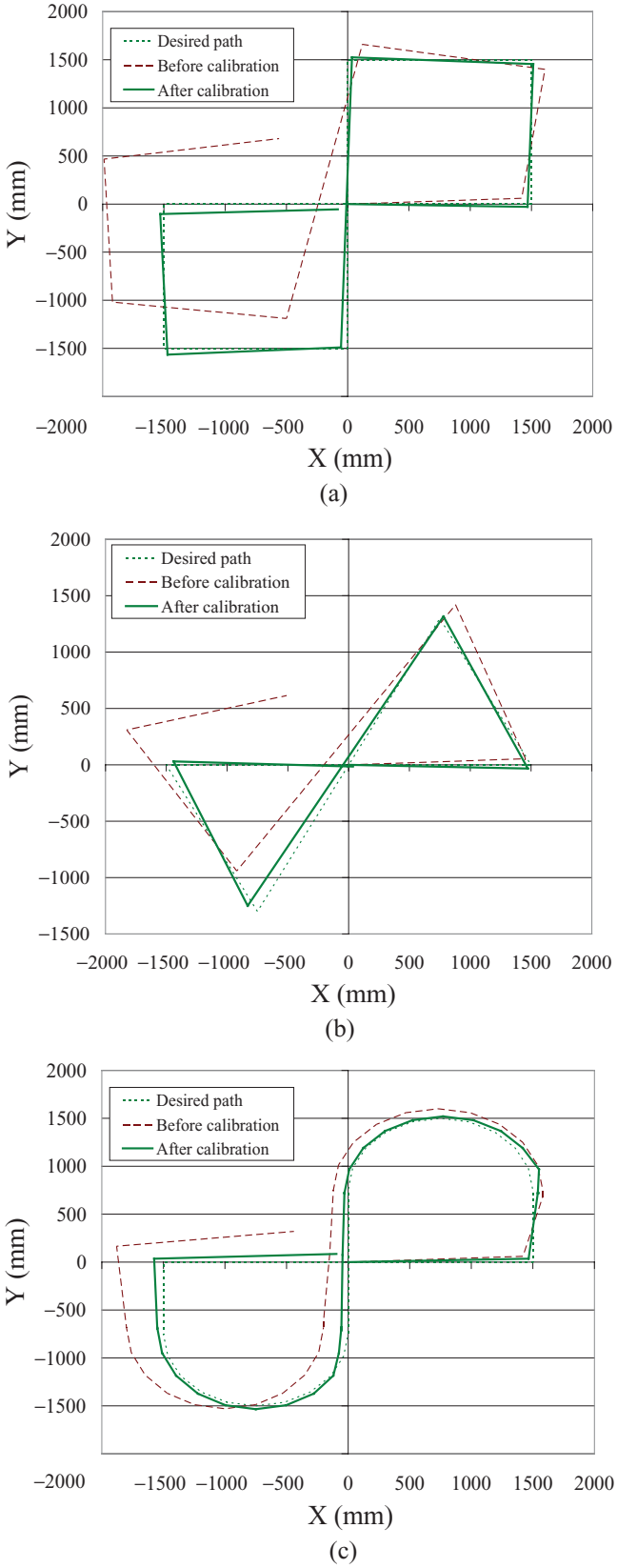

Fig 7. (Colour online) Typical travelled paths along (a) double-square, (b) double-triangular, and (c) combined straight and curved paths.

at which the robot started to move, is shown in Fig. 2(a), and is defined by considering $\alpha_1 = \pi/2$, $\alpha_2 = 7\pi/6$, and $\alpha_3 = 11\pi/6$. The wheels rotated by nominal angular velocity vector is defined as $\dot{\vec{\Phi}}_c = [\,171.90^\circ/\text{s}\ 85.95^\circ/\text{s}\ 85.95^\circ/\text{s}\,]$. The angular velocities, in all tests, were calculated using the kinematic equations defined in Eq. (7). As seen, the robot motion was corrected with the proposed method, i.e., the errors became small after calibration.

Table II illustrates the amount of average errors for this robot before and after calibration as well as estimates of the standard values of skewness and kurtosis using the measured data. The lateral corrective matrix and longitudinal corrective factor are also shown in this table. From Table II, the percentage of error improvement (δr_m) to the variability of data over 10 trials is noticeable (over 84%). The last two columns show the kurtosis and skewness of measured position error. Kurtosis is the measure of the "peakedness" of the probability distribution of a real-valued

https://doi.org/10.1017/S0263574713000210 Published online by Cambridge University Press

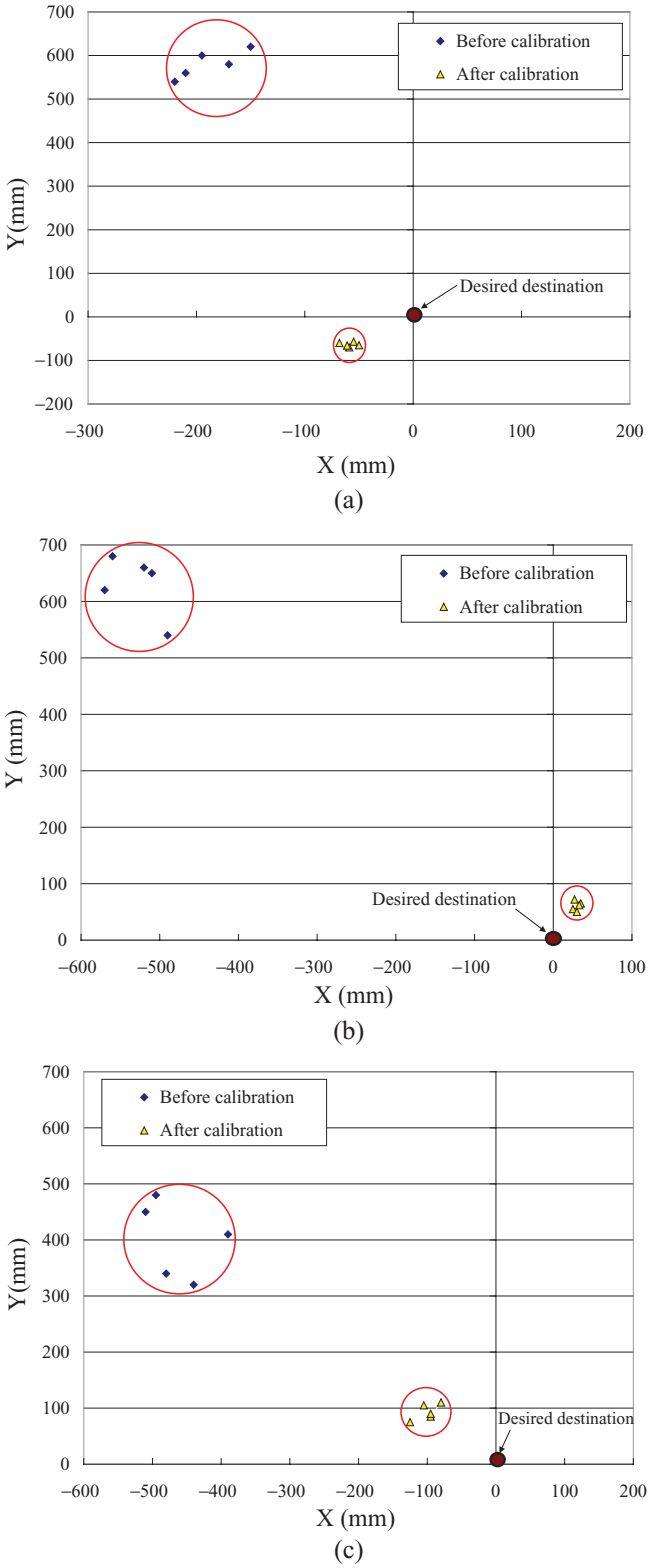

Fig 8. (Colour online) Position of robot in (a) double-square, (b) double-triangular, and (c) combined straight and curved tests.

random variable.[23] Higher kurtosis means more of the probability distribution of a real-valued random variable.[23] The calculated values for the skewness and kurtosis confirm that the derived data satisfy the normal distributions criteria. Note that to justify the normal distribution, calculated absolute values of kurtosis and skewness for certain data group must be less than 2.[12]

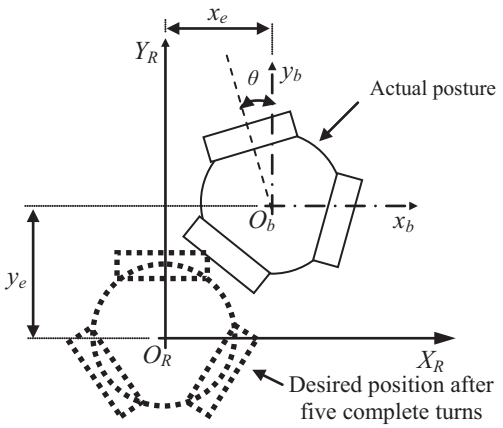

Fig 9. Typical initial, desired, and actual positioning of robot in rotating about central axis.

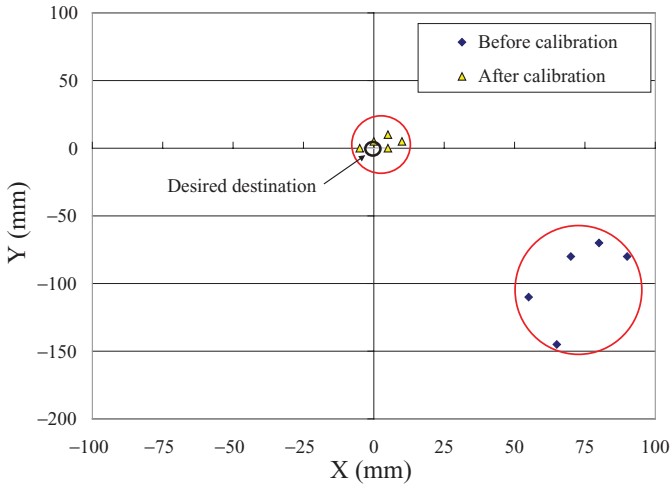

Fig 10. (Colour online) Stop points of robot before and after applying corrective indices in self-rotation.

4.3.2. Validation. In order to validate the workability of the proposed method to correct robot errors, a set of new tests was applied. In this set of tests, the robot was programmed to move along some trajectories consisting of double-square and double-triangular paths, combined straight and curved path, as well as self-rotation. These experiments were done for two different conditions: (i) when the corrective indices (F_{lat} and F_{lon}) were not applied to robot's equations (before calibration), and (ii) when the corrective indices (see Table II) were used (after calibration). In all double-square, double-triangular, and combined straight and curved paths, the length of each straight leg was chosen at 1.5 m and divided into three equal sub-paths used to measure the robot position error during the movement along that path. By marking these points, the position coordinates of robot were measured with respect to the global reference frame, and compared with the ideal values to determine and compare error improvements.

In the following tests, the robot was programmed to follow three unseen trajectories as shown in Fig. 6. Trajectories were designed to allow the robot moving along paths shown in Fig. 6. The robot started at the origin of $X_R Y_R$ coordinate (O_R), labeled "start point," then travelled along the sub-paths to finally return to "O_R." The robot errors,

https://doi.org/10.1017/S0263574713000210 Published online by Cambridge University Press

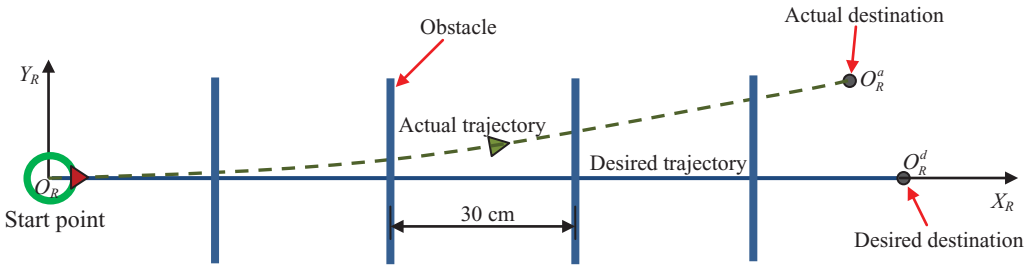

Fig 11. (Colour online) Trajectories in proposed method for non-systematic test. The vertical line shows the artificial obstacle considered to simulate the irregularities during the test run.

Table III. Nominal and corrected wheel angular velocity vectors in double-square test. The nominal velocity vector was applied to robot before calibration. Corrected angular velocity vector was used after calibration.

Sub-paths	Nominal angular velocity (deg/s)	Corrected angular velocity (deg/s)
1 & 8	$[171.9\ -85.9\ -85.9]^T$	$[170.3\ -93.9\ -93.1]^T$
2 & 7	$[0\ 114.6\ -114.6]^T$	$[0\ 125.0\ -124.1]^T$
3 & 6	$[-171.9\ 85.9\ 85.9]^T$	$[-170.3\ 93.9\ 93.1]^T$
4 & 5	$[0\ -114.6\ 114.6]^T$	$[0\ -125.0\ 124.1]^T$

along the sub-paths, are measured with respect to fiducial measurement stations (see solid circles in Fig. 6). The test procedure was done for the prototyped robot and the position coordinates in X- and Y-directions were recorded.

Figures 7(a)–(c) illustrate the desired paths as well as typical actual paths travelled by the robot before and after calibration. These paths are plotted based on the position coordinates recorded in error measurement stations during the robot's motion. As shown, the movement of the robot was corrected for given trajectories after applying the corrective indices. In addition to reduce the radial errors, the proposed method was capable of correcting the path travelled by robot as expected because the test procedure is based on the robot kinematic equations and influences the robot movement along entire path.

Figures 8(a)–(c) depict the actual coordinates of the robot's destinations before and after calibration. As illustrated in all double-square, double-triangular, and combined straight and curved paths, the position error of robot was improved using the proposed calibration method. Using the data from the experiments, it is seen that the root mean square (RMS) values of positioning error were reduced up to 85%, 91%, and 68% in double-square, double-triangular, and combined straight and curved tests, respectively.

Table III illustrates the angular velocity vectors of wheels during travelling along double-square path (as a typical case) before and after applying the corrective indices.

In next test, the robot was programmed to simply rotate about its central axis for five complete turns. In this experiment, all wheels rotated simultaneously with an angular velocity of 1.5 rad/s; therefore, the test investigated the effectiveness of the proposed calibration method when the robot turned about the axis that passed through its center of geometry. As shown in Fig. 9, the uncalibrated robot stops in O_b instead of O_R having three deviations: two longitudinal

Table IV. RMS values of radial position error in systematic test unseen trajectories before (BF) and after (AF) calibration.

Path	δr_e (mm) BF	δr_e (mm) AF	RMS improvement (%)
Double-square	610.9	86.7	85.8
Double-triangular	823.7	67.9	91.8
Combined straight and curved	275.7	86.7	68.6
Central rotation	11.1	0.7	93.7

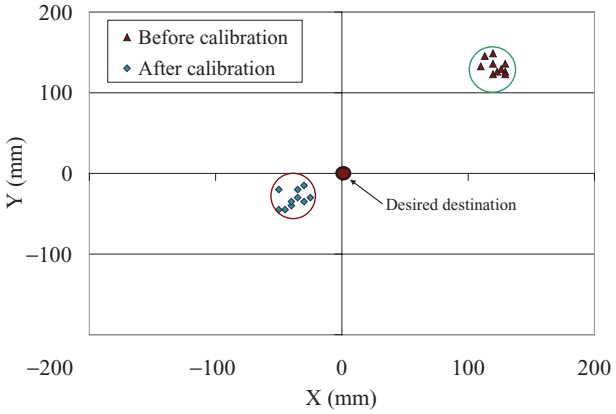

Fig 12. (Colour online) Coordinates of robot's stop point in non-systematic test before and after calibration.

deviations (x_e and y_e) and one orientation deviation (θ). Thus, we should apply the corrective indices, obtained from Table II, to correct the robot motion. Figure 10 shows the final robot position after five times complete rotation.

Table IV illustrates RMS values of the radial position errors of robot along the double-square, double-triangular, combined straight and curved, and self-rotation paths before and after calibration. The RMS values are obtained using the calculated radial position errors during N tests (for all four tests $N = 5$). Also, this table shows the RMS error improvement during the calibration after and before the calibration. As shown in Table IV, the RMS values of position error were improved by at least 85%, 91%, 68%, and 93% along double-square, double-triangular, combined straight and curved paths, and self-rotation, respectively.

4.4. Calibration of non-systematic errors

4.4.1. Calibration process. Non-systematic errors are caused by unpredictable phenomenon such as slippery floors, over acceleration and fast turning, external forces/torques, and

https://doi.org/10.1017/S0263574713000210 Published online by Cambridge University Press

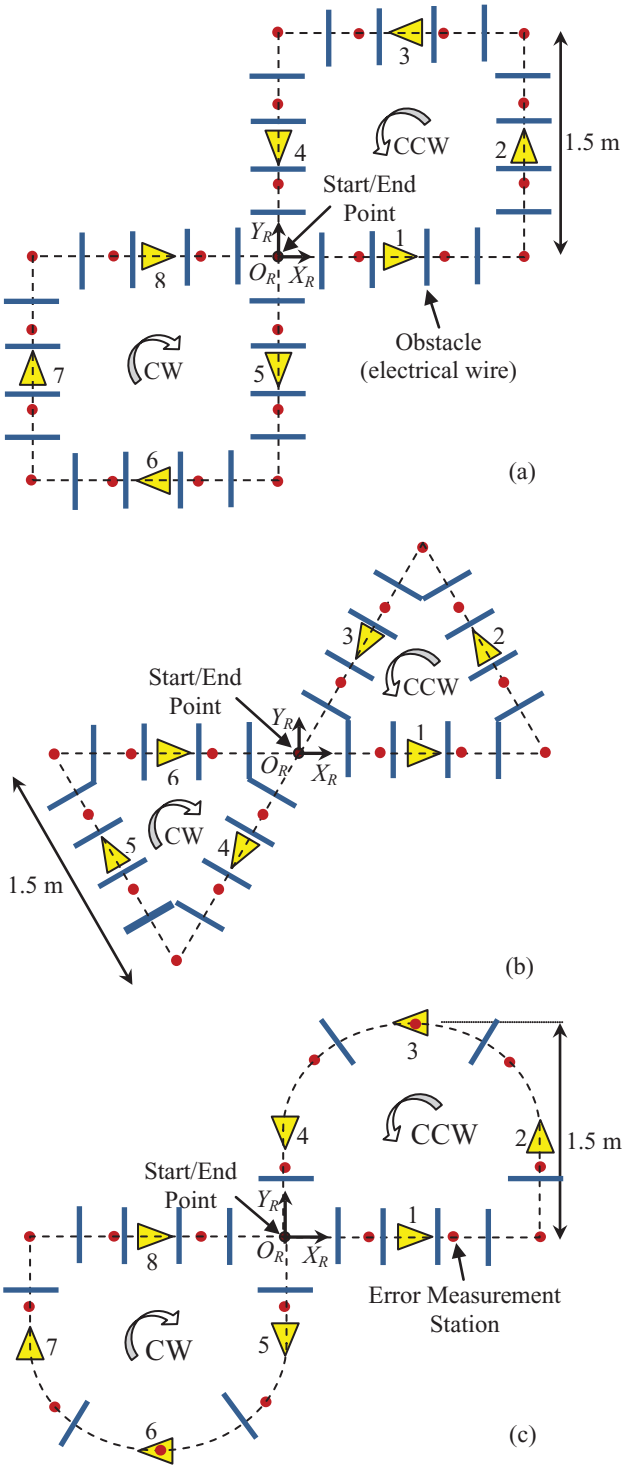

Fig 13. (Colour online) Unseen trajectories for non-systematic error correction tests.

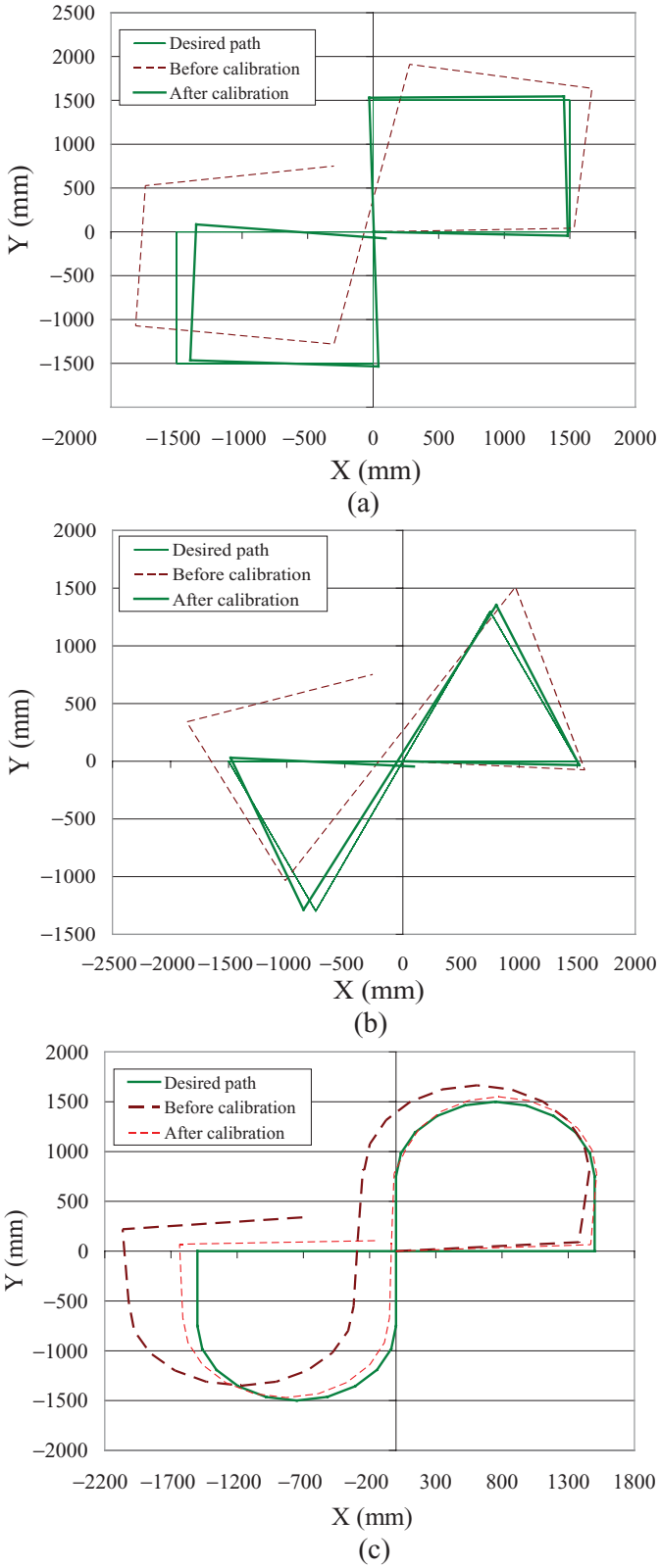

Fig 14. (Colour online) Typical paths: (a) double-square, (b) double-triangular, and (c) combined straight and curved.

non-point wheel contact on the floor. Examples are moving on ice, inaccurate controllers, irregularities on the surface, such as bumps and cracks, and rubber wheels. These phenomena cause the robot wheels to rotate differently with respect to the desired rotation. Thus, the trajectory length travelled by robot changes. These errors are the utmost important problems in real applications. Since it is almost impossible to predict or simulate the exact nature of surface irregularities to which the robot will be exposed, it is difficult to present a general quantitative test procedure for non-systematic errors.[13] Due to the significance of non-systematic error effects on omnidirectional mobile robot's movement, in this section, the compensation of non-systematic errors is investigated by following the methodology described in Section 3. Non-systematic errors are usually modelled by introducing surface irregularities using artificial obstacles

https://doi.org/10.1017/S0263574713000210 Published online by Cambridge University Press

Table V. Indices for non-systematic tests before (BF) and after (AF) calibration.

F'_{lat}	F'_{lon}	δr_e (mm)	δr_m	Kurtosis	Skewness
$diag[\,1.067\ 0.963\ 0.979\,]$	0.909	180.4 (BF) 49.9 (AF)	72.30%	−0.47 (BF) −0.87 (AF)	0.19 (BF) 0.15 (AF)

which can be selected based on the geometry of real working environment of robot.[13] The chosen obstacles for experiments are common electrical cable, such as the ones used in the following experiments, with 5-mm diameter, rounded shape, and plastic coating. The distance between the wires should be chosen based on the condition of real environment. In this work, the cables are evenly placed along the trajectories (see Fig. 11). In the following experiments, the distance is chosen to be 30 mm in each straight leg with no obstacle located on the vertices. The process implemented here is in line with previous study on calibration of non-systematic errors[13] by other researchers. Upon completion the test bed, the sequences described in Section 3, steps (i) to (vii), are implemented. Finally, the non-systematic test corrective indices (F'_{lat} and F'_{lon}) are calculated and the robot is programmed to reduce non-systematic errors. If the environment changes, then values of lateral corrective matrix (F'_{lat}) and longitudinal corrective factor (F'_{lon}) must be adjusted. Towards this goal, the tests should be performed on a platform with the same characteristics of the desired surface on which the robot will be programmed to move after calibration. For instance, if the robot is supposed to move on the carpet, the calibration process should be done on the carpet, or a similar platform.

Figure 12 depicts the coordinate of robot's final position in non-systematic test. The initial configuration of robot is the same as the one described in Fig. 2. As seen, the final position of robot is modified as opposed to position before calibration test.

Table V shows the amount of non-systematic average errors for this robot before and after calibration as well as the non-systematic lateral corrective matrix (F'_{lat}), longitudinal corrective factor (F'_{lon}), and improvement (δr_m). Table V also shows the standard values of skewness and kurtosis using the measured data. The obtained values of skewness and kurtosis indicate that the derived data satisfy the normal distribution criteria. It is obvious that by changing the artificial obstacles geometry or arrangement, the robot's final position and corresponding corrective matrix, and factor might be affected. Consequently, the new lateral corrective matrix and longitudinal corrective factor will be achieved. As shown, the positioning error of the robot was reduced by 72% for the environment with considered obstacles.

4.4.2. Validation . In this set of tests, double-square, double-triangular, and combined straight and curved paths were used to validate the proposed non-systematic test method. The robot travelled along three unseen trajectories using the procedure described in Section 4.3.2 (see Fig. 13). As shown in Fig. 13, the obstacles (thick lines) were made from the rounded shape plastic coating wires, with 5-mm diameter, similar to the calibration tests.

Figures 14(a)–(c) show the desired path and the typical actual paths (before and after calibration) of robot using double-square, double-triangular, and combined straight and curved paths, respectively. As illustrated, the movement of robot was corrected for given paths after applying the corrective parameters (i.e., F'_{lat} and F'_{lon}). It was found that in addition to reduce the final radial error, the proposed method could keep the robot close to desired path. The nominal (before calibration) and corrected (after calibration) angular velocities, in double-square path, are illustrated in Table VI. The RMS values of the position error of the robot are given in Table VII. As shown in Table VII, the RMS values of position error were improved by at least 85%, 86%, and 74% along double-square, double-triangular, and combined straight and curved paths, respectively.

The results show that, in addition to correcting the systematic errors (see Table IV), the method was also able to reduce the non-systematic errors. However, the percentage of error corrections depended on the type of the chosen path, which can be seen from Table VII.

Overall, with reference to Tables IV and VII, it is observed that the proposed method could reduce position errors by at least 68%. The results also show that unseen tests along the combined straight and curved paths are less accurate than any path in which the robot moves along straight trajectory.

Table VIII shows values of the end-point coordinates of robot (in $X_R Y_R$ plane) for tests depicted in Figs. 7 and 14. From the result, for these typical trajectories, position errors were improved in all three unseen paths by at least 70%. Comparing the last column of Table VIII with the ones in

Table VI. Nominal and corrected angular velocities of wheels in double-square path.

Sub-paths	Nominal angular velocity (deg/s)	Corrected angular velocity (deg/s)
1 & 8	$[\,171.9\ -85.9\ -85.9\,]^T$	$[\,183.4\ -82.8\ -84.2\,]^T$
2 & 7	$[\,0\ 114.6\ -114.6\,]^T$	$[\,0\ 110.4\ -112.2\,]^T$
3 & 6	$[\,-171.9\ 85.9\ 85.9\,]^T$	$[\,-183.4\ 82.8\ 84.2\,]^T$
4 & 5	$[\,0\ -114.6\ 114.6\,]^T$	$[\,0\ -110.4\ 112.2\,]^T$

Table VII. RMS values of radial position error along unseen trajectories for non-systematic test before (BF) and after (AF) calibration.

Path	δr_e (mm)		RMS improvement (%)
	BF	AF	
Double-square	808.2	121.0	85.0
Double-triangular	795.67	105.1	86.8
Combined straight and curved	731.4	187.2	74.4

https://doi.org/10.1017/S0263574713000210 Published online by Cambridge University Press

Table VIII. End-point coordinates and error improvement along unseen trajectories before and after calibration for typical trajectories shown in Figs. (7) and (14).

Test	Path	Before calibration	After calibration	δr_m (%)
Systematic test	Double-square	(−560, 670)	(−80, −55)	88.9
	Double-triangular	(−510, 605)	(65, −50)	89.6
	Combined	(−415, 290)	(−110, 105)	70.0
Non-systematic test	Double-square	(−295, 755)	(100, −80)	84.2
	Double-triangular	(−260, 745)	(105, −55)	85.0
	Combined	(−645, 350)	(−165, 110)	73.0

Tables IV and VII, the radial error improvements in both systematic and non-systematic tests are seen within ± 5% of each other.

5. Conclusions

This paper presented a calibration technique for position error reduction of omnidirectional WMR movement. The proposed method was built upon the kinematic equations and Jacobian matrices of omnidirectional mobile robots. The method was implemented to correct positioning errors of a prototyped three-wheeled omnidirectional mobile robot. The calibrated robot was then tested along a number of unseen trajectories. The trajectories were double-square and double-triangular paths, combination of straight and curved paths, as well as self-rotation about central axis. Using statistical indices, it was shown that the proposed method of calibration leads to reasonable error improvement. Specifically, experimental results, using unseen test trajectories, showed that the measured systematic and non-systematic error improvement percentages were enhanced by over 68% and 74%, respectively. The proposed method exhibited more error improvement along double-square and double-triangular paths as compared with curved paths. Specifically, the position errors were reduced by at least 85%, 86% and 68% along double-square, double-triangle, and combined straight and curved paths, respectively. The standard values of skewness and kurtosis from measured data for each test were estimated showing that the derived data satisfy normal distributions criteria. The proposed method is constructed based on the easy-to-understand equations and does not need any knowledge about the sources of robot errors. Furthermore, the method can be used for calibration of mobile robots having omnidirectional wheels as well as all types of WMRs with various numbers of active wheels.

References

1. J. F. Blumrich, *Omnidirectional Vehicle*. United States Patent, No. 3,789,947 (US Patent Office, Alexandria, VA, 1974).
2. B. E. Ilou, *Wheels for a Course Stable Self-Propelling Vehicle Movable in Any Desired Direction on the Ground or Some Other Base*, United States Patent, No. 3,876, 255, (US Patent Office, Alexandria, VA, 1975).
3. M. West and H. Asada, "Design of ball wheel mechanisms for omnidirectional vehicles with full mobility and invariant kinematics," *J. Mech. Des.* **119(2)**, 153–161 (1997).
4. M. Wada and S. Mory, "Holonomic and Omnidirectional Vehicle with Conventional Tires," **In**: *Proceedings of IEEE International Conference on Robotics and Automation* (April 22–28, 1996) pp. 3671–3676.
5. BIPM-JCGM, *International Vocabulary of Metrology–Basic and General Concepts and Associated Terms* (VIM), 3rd ed., JCGM 200:2008 (BIPM-JCGM, Cedex, France, 2008), pp. 16–34.
6. Y. Maddahi and A. Maddahi, "Mobile Robots Experimental Analysis Based on Kinematics," **In**: *Proceedings of the International Conference on Simulation, Modeling and Optimization*, Turkey (2004) pp.1662–1667.
7. K. Jung-Hwan, H. Dong-Choon, J. Yong-Woo and K. Eun-Soo, "Intelligent Mobile Robot System for Path Planning Using Stereo Camera-Based Geometry Information," **In**: *Proceeding of SPIE – International Society for Optical Engineering*, *Optical Metrology*: vol. 6006, Boston, Massachusetts (2005) pp. 232–243.
8. M. Piaggio, A. Sgorbissa and R. Zaccaria, "Navigation and localization for service mobile robots based on active beacons," *J. Syst. Sci.* **27**(4), 71–83 (2001).
9. B. Bury and J. C. Hope, "Autonomous Mobile Robot Navigation Using a Low-cost Fibre Optic Gyroscope," **In**: *Proceeding of the International Conference on Intelligent Autonomous Vehicles*, Espoo, Finland (1995) pp. 39–43.
10. W. Kwon, K. S. Roh and H. K. Sung, "Particle Filter-Based Heading Estimation Using Magnetic Compasses for Mobile Robot Navigation," **In**: *Proceedings of the International Conference on Robotics and Automation*, Orlando, Florida (May 15–19, 2006) pp. 2705–2712.
11. N. Roy and S. Thrun, "Online Self-Calibration for Mobile Robots," **In**: *Proceedings of the IEEE International Conference on Robotics and Automation*, vol. 3, Detroit, Michigan (May 10–15, 1999) pp. 2292–2297.
12. Y. Maddahi, N. Sepehri, A. Maddahi and M. Abdolmohammadi, "Calibration of wheeled mobile robots with differential drive mechanisms: An experimental approach," *J. Robot.* **30**(6), 1029–1039 (2012).
13. J. Borenstein and L. Feng, "UMBmark: A Benchmark Test for Measuring Dead reckoning Errors in Mobile Robots," **In**: *Proceedings of the SPIE Conference on Mobile Robots*, Newton, Massachusetts (1995) pp. 178–186.
14. J. Borenstein and L. Feng, "UMBmark: A Method for Measuring, Comparing, and Correcting Dead-Reckoning Errors in Mobile Robots," *Technical Report* (The University of Michigan UM-MEAM-94–22, 1994).
15. J. Borenstein and L. Feng, "Measurement and correction of systematic odometry errors in mobile robots," *IEEE Trans. Intell. Robots Syst.* **12**(6), 869–880 (1996).
16. Y. Maddahi, "Design and Laboratory Tests of Wheeled Mobile Robots," **In**: *International Conference on System Science and Simulation in Engineering*, Tenerife, Spain (2005) pp. 186–191.
17. K. H. Han, H. K. Kin and J. S. Lee, "The Sources of Position Errors of Omni-Directional Mobile Robot with Mecanum Wheel," **In**: *IEEE International Conference on Systems, Man and Cybernetics*, Piscataway, New Jersey (2010) pp. 581–586.

https://doi.org/10.1017/S0263574713000210 Published online by Cambridge University Press

18. J.-H Lee and H. Hashimoto, "Controlling mobile robots in distributed intelligent sensor network," *IEEE Trans. Ind. Electron.* **50**(5), 890–902 (2003).
19. P. T. Szemes, H. Hashimoto and P. Korondi, "Pedestrian-behavior-based mobile agent control in intelligent space," *IEEE Trans. Instrum. Meas.* **54**(6), 2250–2257 (2005).
20. R. Tsai, "A versatile camera calibration technique for high accuracy 3D machine vision metrology using off-the-shelf TV cameras and lenses," *IEEE Trans. Robot. Automat.* **3**, 323–344 (1987).
21. W.-C. Chang and P.-R. Chu, "An Intelligent Space for Mobile Robot Navigation with On-line Calibrated Vision Sensors," **In**: *International Conference on Control, Automation, Robotics and Vision*, Singapore (Dec 7–10, 2010) pp. 1452–1457.
22. R. Siegwart and I. R. Nourbakhsh, *Introduction to Autonomous Mobile Robots* (MIT Press, Cambridge, Massachusetts, 2004).
23. K. L. Wuensch, *Encyclopedia of Statistics in Behavioral Science* (Wiley, Chichester, UK, 2005).

https://doi.org/10.1017/S0263574713000210 Published online by Cambridge University Press